Spin-Orbit Coupling and the Optical Spin Hall Effect in Photonic Graphene

A. V. Nalitov, G. Malpuech, H. Terças, and D. D. Solnyshkov
Institut Pascal, PHOTON-N2, Clermont Université, Blaise Pascal University, CNRS, 24 avenue des Landais, 63177 Aubière Cedex, France
(Received 25 April 2014; published 16 January 2015)

We study the spin-orbit coupling induced by the splitting between TE and TM optical modes in a photonic honeycomb lattice. Using a tight-binding approach, we calculate analytically the band structure. Close to the Dirac point, we derive an effective Hamiltonian. We find that the local reduced symmetry (D_{3h}) transforms the TE-TM effective magnetic field into an emergent field with a Dresselhaus symmetry. As a result, particles become massive, but no gap opens. The emergent field symmetry is revealed by the optical spin Hall effect.

DOI: 10.1103/PhysRevLett.114.026803 PACS numbers: 73.22.Pr, 71.36.+c, 78.67.Wj

Spin-orbit coupling (SOC) in crystals allows us to create and control spin currents without applying external magnetic fields. These phenomena were described in the 1970s [1] and are nowadays called the spin Hall effect (SHE) [2,3]. In 2005, the interplay between the SOC and the specific crystal symmetry of graphene [4] was proposed [5] to be at the origin of a new type of spin Hall effect, the quantum spin Hall effect, in which the spin currents are supported by surface states and are topologically protected [6,7]. This result has special importance, since it defines a new class of Z_2-topogical insulator [8], not associated with the quantization of the total conductance, but associated with the quantization of the spin conductance. However, from an experimental point of view, the realization of any kind of SHE is difficult, because SOC does not only lead to the creation of spin current, but also to spin decoherence [9]. In graphene, the situation is even worse, since the SOC is extremely weak. Deposition of adatoms has been proposed to increase the SOC [10], and it allowed the recent observation of the SHE [11], but associated with a very short spin relaxation length, of the order of 1 μm.

On the other hand, artificial honeycomb lattices for both bosonic [12], fermionic atoms [13], and photons [14–18] have been realized. These systems are gaining a lot of attention due to the large possible control over the system parameters, up to complete Hamiltonian engineering [19,20]. In atomic systems, the recent implementation of synthetic magnetic fields [21] and non-Abelian, Rashba-Dresselhauss gauge fields [22] appears promising in view of the achievement of topological insulator analogs. Recent experimental advances in atomic physics include the use of the Aharanov-Bohm effect to measure topology [23] and the implementation of the Haldane model [24]. Photonic systems, and specifically photonic honeycomb lattices, are quite promising as well. They are based on coupled wave guide arrays [25], photonic crystals with honeycomb symmetry [26], and etched planar cavities [18], and other structures with periodic potentials for photons [27,28]. A photonic Floquet topological insulator has been recently reported [29], and some others based on the magnetic response of metamaterials [30], polaritons [31–33], and indirect excitons [33] are predicted. In photonic systems, SOC naturally appears from the energy splitting between the TE and TM optical modes [34] and from structural anisotropies [35]. Both effects can be described in terms of effective magnetic fields acting on the photon (pseudo)spin [36]. In planar cavity systems, the TE-TM effective field breaks the rotational symmetry but preserves both time reversal and spatial inversion symmetries. It is characterized by a k^2 scaling and a double azimuthal dependence. This SOC is at the origin of the optical spin Hall effect (OSHE) [37,38] and the acceleration of effective magnetic monopoles [39–41]. As was recently shown [42], the specific TE-TM symmetry can be locally transformed into a non-Abelian gauge field in a structure with a reduced spatial symmetry. In etched planar cavities, the TE-TM splitting is still present, but it is reinforced by strain and other structural effects that enhance splittings [35,43–45] which can reach hundreds of μeV.

In this work, we calculate the band structure of photonic graphene in the presence of the intrinsic SOC induced by the TE-TM splitting. We derive an effective Hamiltonian that allows us to extract an effective magnetic field acting on the photon pseudospin only. We find that the low symmetry (D_{3h}) induced by the honeycomb lattice close to the Dirac points transforms the TE-TM field in an emergent field with a Dresselhaus symmetry. Particles become massive, but no gap opens. The dispersion topology shows large similarities with the one of bilayer graphene [46] and of monolayer graphene with Rashba SOC [47], featuring trigonal warping [48]. The symmetry of these states is revealed by the OSHE, which we describe by simulating resonant optical excitation of the Γ, K, and K' points. The OSHE at the Γ point shows four spin domains associated with the TE-TM symmetry. The OSHE at K and K' shows two domains characteristic of the Dresshlauss symmetry. The spin domains at the K and K' points are inverted, which is a signature of the restored D_{6h} symmetry when the two valleys are included.

In what follows, in order to be specific, we consider a honeycomb lattice based on a patterned planar microcavity similar to the one recently fabricated and studied [18]. This does not reduce the generality of our description, which can apply to other physical realizations of honeycomb lattices, in optical and nonoptical systems. In Ref. [18], quantum wells were embedded in the cavity which provided the strong coupling regime and the formation of cavity exciton polaritons. Here, we will consider the linear regime, a parabolic in-plane dispersion, and no applied magnetic field. In such a case, photons and exciton polaritons behave in a similar way, and our formalism applies to both types of particles.

Tight-binding model.—First, we describe the SOC in a photonic graphene structure [Fig. 1(a)] within the tight-binding approximation. We take a basis of $\sigma\pm$ polarized photon states localized on each pillar of the lattice as a zeroth approximation for the tight-binding model and introduce the hopping of photons from a pillar to one of its nearest neighbors as a perturbation.

To illustrate the polarization dependence of the hopping probability, let us consider two neighboring pillars A and B, shown in Fig. 1(b). The photon hopping between them may be described as propagation through a "waveguidelike" link. TE-TM energy splitting imposes a slight difference δJ in tunneling matrix elements for states linearly polarized longitudinally (L) and transversely (T) to vector $\mathbf{d}_\varphi$ linking the pillars [49], as it was recently shown for the eigenstates in a photonic benzene molecule [45]. In that framework, the matrix elements read: $\langle A,L|\hat{V}|B,L\rangle \equiv -J-\delta J/2$, $\langle A,T|\hat{V}|B,T\rangle \equiv -J+\delta J/2$. While a photon is in a link, the TE-TM field does not rotate its eigenstate polarizations L and T, implying no cross-polarization matrix elements:

$$\langle A,L|\hat{V}|B,T\rangle = \langle A,T|\hat{V}|B,L\rangle = 0.$$

In $\sigma\pm$ basis, the probability of spin flip during hopping is linear in δJ and its phase gain depends on the angle φ between the link and the horizontal axis:

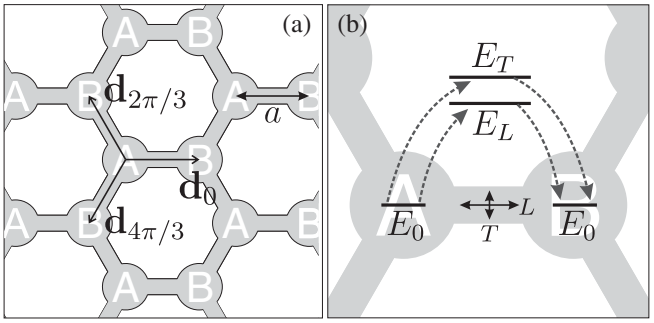

FIG. 1. A schematic sketch of the tight-binding model. (a) Photon tunneling between microcavity pillars is described as photon propagation through "waveguidelike" links. (b) Polarization dependence of tunneling probability due to TE-TM energy splitting: L state which is polarized longitudinally to the "waveguide" link is closer in energy to the degenerate pillar-pinned states than the transversely polarized state T, resulting in higher L-photon tunneling probability through the link.

$$\langle A,\pm|\hat{V}|B,\pm\rangle = -J, \qquad \langle A,+|\hat{V}|B,-\rangle = -\delta J e^{-2i\varphi}.$$

This phase factor reflects the fact that when a link is rotated by 90 deg, the L and T polarization basis is inverted: if L was horizontal, it becomes vertical and vice versa.

A photon state may be described in the bispinor form $\Phi = (\Psi_A^+, \Psi_A^-, \Psi_B^+, \Psi_B^-)^T$, with $\Psi_{A(B)}^\pm$ being the wave function on both sublattices in both spin components. The effective Hamiltonian acting on a plane wave bispinor $\Phi_\mathbf{k}$ then has a block matrix form:

$$\mathrm{H}_\mathbf{k} = \begin{pmatrix} 0 & \mathrm{F}_\mathbf{k} \\ \mathrm{F}_\mathbf{k}^\dagger & 0 \end{pmatrix}, \qquad \mathrm{F}_\mathbf{k} = -\begin{pmatrix} f_\mathbf{k} J & f_\mathbf{k}^+ \delta J \\ f_\mathbf{k}^- \delta J & f_\mathbf{k} J \end{pmatrix}, \tag{1}$$

where complex coefficients $f_\mathbf{k}$, $f_\mathbf{k}^\pm$ are defined by

$$f_\mathbf{k} = \sum_{j=1}^{3} \exp(-i\mathbf{k}\mathbf{d}_{\varphi_j}), \quad f_\mathbf{k}^\pm = \sum_{j=1}^{3} \exp(-i[\mathbf{k}\mathbf{d}_{\varphi_j} \mp 2\varphi_j]),$$

and $\varphi_j = 2\pi(j-1)/3$ is the angle between the horizontal axis and the direction to the jth nearest neighbor of a type-A pillar. Its diagonalization results in a biquadratic equation on the photon dispersion, having two pairs of solutions $\pm E_\mathbf{k}^\pm$, given by

$$2(E_\mathbf{k}^\pm)^2 = 2|f_\mathbf{k}|^2 J^2 + (|f_\mathbf{k}^+|^2 + |f_\mathbf{k}^-|^2)\delta J^2 \pm \sqrt{(|f_\mathbf{k}^+|^2 - |f_\mathbf{k}^-|^2)^2 \delta J^4 + 4|f_\mathbf{k} f_\mathbf{k}^{+*} + f_\mathbf{k}^* f_\mathbf{k}^-|^2 J^2 \delta J^2}. \tag{2}$$

The graphenelike energy dispersion is plotted along the principal direction in Fig. 2(a) for $\delta J/J = 0.1$. The trigonal warping effect, which consists of the emergence of three additional Dirac cones in the vicinity of each of the K and K' points, is shown in Fig. 2(b). It occurs as well in bilayer graphene [46] and in monolayer graphene with Rashba SOC [47]. If $\delta J \ll J$, the distance δK between a Dirac point and additional pockets is approximately given by $(\delta J/J)^2 a^{-1}$. When $\delta J = J/2$, a transition of the dispersion topology occurs: the additional Dirac points originating from K and K' meet at the M point and annihilate.

The effective Hamiltonian may be formulated in terms of pseudospin operators $\boldsymbol{\sigma}$ and $\mathbf{s}$, having the same matrix form of Pauli vector and corresponding to sublattice (A/B) and polarization degrees of freedom. It may further be separated into a polarization-independent part $H_\mathbf{k}^{(0)}$, coupling $\boldsymbol{\sigma}$ with momentum and giving a standard graphene dispersion with two Dirac valleys K and K', and a spin-orbit term $H_\mathbf{k}^{\mathrm{SO}}$, coupling $\mathbf{s}$ with $\boldsymbol{\sigma}$ and momentum:

$$H_\mathbf{k}^{(0)} = -J\sigma_+ f_\mathbf{k} + \mathrm{H.c.}, \tag{3}$$

$$H_\mathbf{k}^{\mathrm{SO}} = -\delta J \sigma_+ \otimes (f_\mathbf{k}^+ s_+ + f_\mathbf{k}^- s_-) + \mathrm{H.c.}, \tag{4}$$

where $\sigma_\pm = (\sigma_x \pm i\sigma_y)/2$, $s_\pm = (s_x \pm i s_y)/2$, and the $\otimes$ symbol denotes the Kronecker product. Expanding expressions (3) and (4) and keeping the first order in $\mathbf{q} = \mathbf{k} - \mathbf{K}$, we

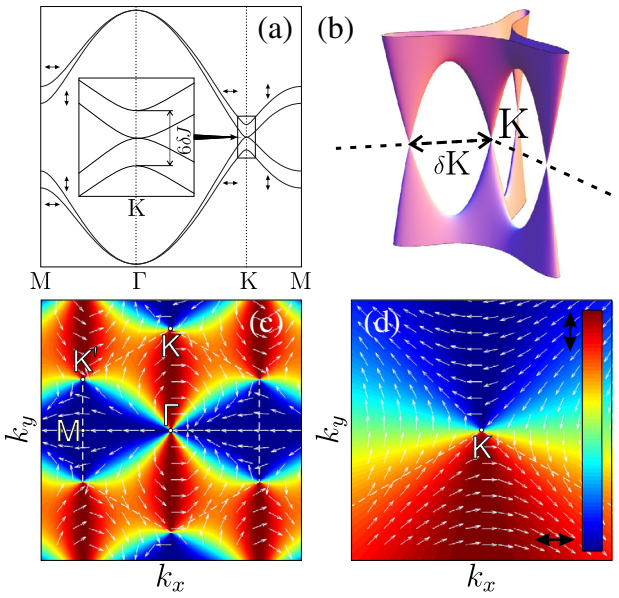

FIG. 2 (color online). The eigenenergies and eigenstate polarizations of the polariton graphene Hamiltonian. (a) Photon energy dispersion branches along principal directions. The inset demonstrates a zoomed K valley—the dispersion is gapless. Horizontal and vertical double arrows represent the linear polarization of eigenstates along x and y axes, respectively. (b) A sketch of the trigonal warping effect: $E_{\mathbf{k}}^{-}$ pair of dispersion branches has four Dirac points in the vicinity of each zone corner. (c), (d) In-plane light polarization map shown by the colors and the corresponding pseudospin texture (shown by the arrows) of the lowest energy state.

further isolate the momentum-independent and -dependent parts $H_{\mathbf{K}}^{\mathrm{SO}}$ and $H_{\mathbf{q}}^{\mathrm{SO}}$ to finally rewrite all terms in the low-energy approximation:

$$H_{\mathbf{q}}^{(0)} = \hbar v_F(\tau_z q_x \sigma_x + q_y \sigma_y), \tag{5}$$

$$H_{\mathbf{K}}^{\mathrm{SO}} = \Delta(\tau_z \sigma_y s_y - \sigma_x s_x), \tag{6}$$

$$H_{\mathbf{q}}^{\mathrm{SO}} = \frac{\Delta a}{2}[s_x(\tau_z q_y \sigma_y - q_x \sigma_x) - s_y(\tau_z q_x \sigma_y + q_y \sigma_x)], \tag{7}$$

where $v_F = 3Ja/(2\hbar)$, $\Delta = 3\delta J/2$, and τ_z equals $+1$ and -1 for K and K' valleys, respectively. Here we use the same basis as the one of Kane and Mele [5] in order to allow a direct comparison with their Hamiltonian. This basis is different from the original basis of Wallace [50], which is used in Eq. (1). The passage from Wallace to Kane is obtained by writing $q_x \to q_y$, $q_y \to -q_x$).

The term (6), similar to the Rashba term introduced by Kane and Mele [5,8], is dominant in the region of reciprocal space where $qa \ll \delta J/J$ and is responsible for the band splitting at K and K'. The interplay between Eqs. (5) and (6) produces an effective photon mass $m^* = \pm(2\hbar^2\delta J)/(3a^2J^2)$ in this region.

Provided $\delta J \ll J$, term (6) still dominates term (7) in the region $\delta J/J \ll qa \ll 1$, but plays a role of perturbation over the polarization-independent graphenelike term (5), splitting its linearly polarized eigenstates in energy. It therefore may be interpreted as an interaction with an emergent in-plane effective magnetic field in this region. Considering either positive ($c = +1$) or negative ($c = -1$) energy states, the spin-orbit term (6) describes the interaction of a polariton with a symmetry-allowed Dresselhaus-like emergent field:

$$H_c^{\mathrm{SO}} = -\Delta c \tau_z (q_x s_x - q_y s_y)/q. \tag{8}$$

The effective field described by the spin-orbit term (8) splits the degenerate massless Dirac cones by $3\delta J$, and their linear polarization only depends on the direction of $\mathbf{q}$ and not on its absolute value. The pseudospin pattern (defining the linear polarization of light, and not associated with the sublattices degree of freedom) of the lowest energy eigenstate reflects the effective field acting on the particles, because the pseudospin aligns with this field. This pattern is plotted with white arrows over the Brillouin zone in Fig. 2(c). Figure 2(d) shows a zoom on the K point where the emergent Dressehlaus-like field is clearly identified. The color in Figs. 2(c) and 2(d) represents the linear polarization degree in the x-y basis, or the pseudospin projection on the x axis. Figure 2(c) also clearly shows that the effective fields have an opposite sign close to the K and K' points, respectively. The first two terms (5) and (6) produce two touching parabolic dispersion branches at K and K', and the third term (7) of the expansion is needed to obtain the trigonal warping effect in the low-energy approximation.

From the dispersion calculations, we can conclude that the particular type of SOC considered here does not open a gap but leads to the appearance of massive particles. At the K, K' points, the in-plane linear polarization degree vanishes. At the K point, the states fully project on Ψ_A^- and Ψ_B^+, respectively, whereas at the K' point they project on Ψ_A^+ and Ψ_B^-, respectively. The induced dissymmetry between K and K' could be revealed by the Faraday effect [51] or Zeeman splitting [31,32], leading to the formation of quantum Hall state analogs. Another consequence is the strong modification of the Klein tunneling effect. As shown in Ref. [52], Klein tunneling is suppressed in the presence of Rashba SOC, since the dispersion is no longer linear at the K point.

The best evidence of the presence of a SOC inducing an effective magnetic field of a specific symmetry is the optical spin Hall effect: rotation of the particle spin around the effective wave-vector-dependent field during their propagation. The resonant excitation around the Γ point with linearly polarixed light should lead to a radial expansion of the wave packet accompanied by a precession of the photon pseudospin. The double azimuthal dependence of the effective field orientation should lead, as in the planar case, to the formation of four spin domains [37,53]. Close to the K and K' points, the Dressehlaus effective field orientation follows the azimuthal angle and only two spin domains should form [42,54].

Numerical simulation.—In the following, in order to check the validity of the tight-binding approximation, and the observability of the OSHE, in realistic structures and experiments, namely, including the broadening induced by

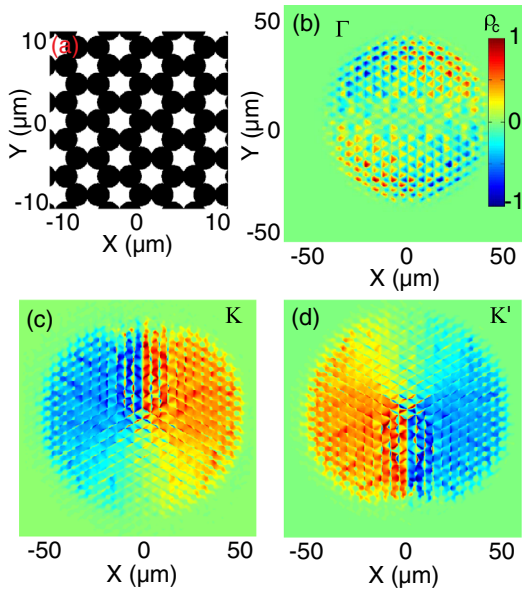

FIG. 3 (color online). Optical spin Hall effect in photonic graphene. Circular polarization degree as a function of coordinates: (a) the potential used in the simulations; (b) excitation at Γ point (TE-TM field); (c) excitation at K point (Dresselhaus effective field); (d) excitation at K' point (field inverted with respect to K').

the finite lifetime, we study numerically the propagation of polarized light in the photonic graphene structure. We consider a structure etched out of a planar microcavity, where the graphene atoms are represented by overlapping pillars [Fig. 3(a)]. The equation of motion for the photonic spinor wave function reads

$$i\hbar\frac{\partial\psi_{\pm}}{\partial t} = -\frac{\hbar^2}{2m}\Delta\psi_{\pm} + U\psi_{\pm} - \frac{i\hbar}{2\tau}\psi_{\pm} + \beta\left(\frac{\partial}{\partial x} \mp i\frac{\partial}{\partial y}\right)^2\psi_{\mp} + P_0 e^{-(t-t_0)^2/\tau_0^2} e^{-(\mathbf{r}-\mathbf{r}_0)^2/\sigma^2} e^{i(\mathbf{kr}-\omega t)}, \quad (9)$$

where $\psi_+(r), \psi_-(r)$ are the two circular components of the photon wave function, m is the cavity photon mass, $\tau =$ 25 ps is the lifetime. This equation is similar to the one describing the photon motion in a planar cavity in the presence of TE-TM splitting [36], described by the parameter $\beta = \hbar^2(m_l^{-1} - m_t^{-1})/4m$, where $m_{l,t}$ are the effective masses of TM and TE polarized particles, respectively, and $m = 2(m_t - m_l)/m_t m_l$. We have taken $m_t = 5 \times 10^{-5} m_0$, $m_l = 0.95 m_t$, where m_0 is the free electron mass. The only difference lies in the introduction of the honeycomb lattice potential $U(r)$ shown in Fig. 3(a) (24×24 elementary cells). P_0 is the amplitude of the pulsed pumping (identical for both components, corresponding to horizontal polarization), the pulse duration is $\tau_0 = 1$ ps, the size of the spot $\sigma = 15$ μm. Pumping is localized in real space and in reciprocal space close to the selected point (Γ, K, or K'). We have performed numerical simulation of the optical spin Hall effect in photonic graphene using a high-resolution (512×512) representation of a potential, similar to the one already studied in experiments [18]. The nVidia CUDA graphical processor was used to carry out the integration of the 2D spinor Schrödinger equation.

Figures 3(b)–3(d) show snapshots taken at $t = 30$ ps of the circular polarization degree as a function of coordinates. Figure 3(b) shows the polarization degree for the excitation in the Γ point, where the field has the typical TE-TM texture, evidenced by the four polarization domains [37,38,53]. Figures 3(c) and 3(d) demonstrate the optical spin Hall effect for the K and K' points, respectively, where the field has the texture of the Dresselhaus SOC. This is evidenced by two polarization domains in real space [42,54] being inverted between the K and K' points because the fields around K and K' are respectively opposite. The OSHE texture is a demonstration of the different nature of the effective SOC field at the two Dirac points K and K'. From this numerical experiment, we clearly see the advantage of photonic systems in comparison to solid-state systems, which allow us to excite and analyze any point of the dispersion with much more facility. Another very interesting consequence of our work relies on the possibilities offered (i) by the manipulation of the lattice geometry and (ii) by the hybrid exciton-photon nature of the polaritons. The same system geometry has been used to create a photonic topological insulator [25]. Combined with SOC, it paves the way for very broad applications. For example, the mixed nature of exciton polaritons provides a magnetic response of the system at optical frequencies, which is of interest to realize a photonic topological insulator [31,32,51,55]. Moreover, polariton-polariton interactions, resulting in strong nonlinear optical response, allow the exploration of quantum light with spin-anisotropic interactions [36,56]. Nonlinear OSHE associated with the transmutation of topological defects and focusing of spin currents has already been described in planar structures [53]. The behavior of soliton states in photonic topological insulators was recently considered [57]. Polaritonic graphene [18] therefore opens very large possibilities for the studies of interacting spinor quantum fluids, in the presence of different types of real and effective magnetic fields, which suggests accessibility to various quantum phases.

To conclude, we have studied the spin-orbit coupling induced by the TE-TM splitting in a microcavity etched in the shape of a graphene lattice. Within the tight-binding approximation, we calculated the eigenstates of the system, derived an effective Hamiltonian, and found the effective field acting on the photon spin. The symmetry of the field is lowered close to the Dirac points where it takes the form of a Dressehlauss field. The experimental observability of OSHE induced by this SOC is verified by numerical simulations.

We acknowledge discussions with M. Glazov, A. Amo, I. Carusotto, and J. Bloch. This work has been supported by the EU ITN INDEX (Grant No. 289968), ANR Labex GANEX (Grant No. ANR-11-LABX-0014), ANR Quandyde (Grant No. ANR-11-BS10-001), and EU IRSES POLAPHEN (Grant No. 246912).

[1] M. I. D'Yakonov and V. I. Perel', JETP Lett. **13**, 467 (1971).
[2] J. E. Hirsch, Phys. Rev. Lett. **83**, 1834 (1999).
[3] Y. K. Kato, R. C. Myers, A. C. Gossard, and D. D. Awschalom, Science **306**, 1910 (2004).
[4] A. K. Geim and K. S. Novoselov, Nat. Mater. **6**, 183 (2007).
[5] C. L. Kane and E. J. Mele, Phys. Rev. Lett. **95**, 226801 (2005).
[6] M. Koenig, S. Wiedmann, C. Bruene, A. Roth, H. Buhmann, L. W. Molenkamp, X.-L. Qi, and S.-C. Zhang, Science **318**, 766 (2007).
[7] M. Z. Hasan and C. L. Kane, Rev. Mod. Phys. **82**, 3045 (2010).
[8] C. L. Kane and E. J. Mele, Phys. Rev. Lett. **95**, 146802 (2005).
[9] M. Dyakonov and V. Perel, Sov. Phys. Solid State **13**, 3023 (1972).
[10] M. Gmitra, D. Kochan, and J. Fabian, Phys. Rev. Lett. **110**, 246602 (2013).
[11] J. Balakrishnan, G. Kok Wai Koon, M. Jaiswal, A. H. Castro Neto, and B. Ozyilmaz, Nat. Phys. **9**, 284 (2013).
[12] P. Soltan-Panahi, J. Struck, P. Hauke, A. Bick, W. Plenkers, G. Meineke, C. Becker, P. Windpassinger, M. Lewenstein, and K. Sengstock, Nat. Phys. **7**, 434 (2011).
[13] L. Tarruell, D. Greif, T. Uehlinger, G. Jotzu, and T. Esslinger, Nature (London) **483**, 302 (2012).
[14] O. Peleg, G. Bartal, B. Freedman, O. Manela, M. Segev, and D. N. Christodoulides, Phys. Rev. Lett. **98**, 103901 (2007).
[15] U. Kuhl, S. Barkhofen, T. Tudorovskiy, H.-J. Stöckmann, T. Hossain, L. de Forges de Parny, and F. Mortessagne, Phys. Rev. B **82**, 094308 (2010).
[16] M. Polini, F. Guinea, M. Lewenstein, H. C. Manoharan, and V. Pellegrini, Nat. Nanotechnol. **8**, 625 (2013).
[17] E. Kalesaki, C. Delerue, C. Morais Smith, W. Beugeling, G. Allan, and D. Vanmaekelbergh, Phys. Rev. X **4**, 011010 (2014).
[18] T. Jacqmin, I. Carusotto, I. Sagnes, M. Abbarchi, D. D. Solnyshkov, G. Malpuech, E. Galopin, A. Lemaitre, J. Bloch, and A. Amo, Phys. Rev. Lett. **112**, 116402 (2014).
[19] M. Hafezi, E. Demler, M. Lukin, and J. Taylor, Nat. Phys. **7**, 907 (2011).
[20] R. O. Umucalilar and I. Carusotto, Phys. Rev. Lett. **108**, 206809 (2012).
[21] Y.-J. Lin, R. L. Compton, K. Jimenez-Garcia, J. V. Porto, and I. B. Spielman, Nature (London) **462**, 628 (2009).
[22] Y.-J. Lin, K. Jimenez-Garcia, and I. B. Spielman, Nature (London) **471**, 83 (2011).
[23] L. Duca, T. Li, M. Reitter, I. Bloch, M. Schleier-Smith, and U. Schneider, Science, doi:10.1126/science.1259052 (2014).
[24] G. Jotzu, M. Messer, R. Desbuquois, M. Lebrat, T. Uehlinger, D. Greif, and T. Esslinger, Nature (London) **515**, 237 (2014).
[25] M. Rechtsman, J. Zeuner, Y. Plotnik, Y. Lumer, D. Podolsky, F. Dreisow, S. Nolte, M. Segev, and A. Szameit, Nature (London) **496**, 196 (2013).
[26] R. Won, Nat. Photonics **5**, 512 (2011).
[27] N. Y. Kim, K. Kusudo, C. Wu, N. Masumoto, A. Loffler, S. Hofling, N. Kumada, L. Worschech, A. Forchel, and Y. Yamamoto, Nat. Phys. **7**, 681 (2011).
[28] E. A. Cerda-Méndez, D. Sarkar, D. N. Krizhanovskii, S. S. Gavrilov, K. Biermann, M. S. Skolnick, and P. V. Santos, Phys. Rev. Lett. **111**, 146401 (2013).
[29] Y. Chong, Nature (London) **496**, 173 (2013).
[30] A. Khanikaev, S. Mousavi, W.-K. Tse, M. Kargarian, A. MacDonald, and G. Shvets, Nat. Mater. **12**, 233 (2013).
[31] T. Karzig, C.-E. Bardyn, N. Lindner, and G. Refael, arXiv:1406.4156.
[32] A. Nalitov, D. Solnyshkov, and G. Malpuech, arXiv:1409.6564.
[33] C.-E. Bardyn, T. Karzig, G. Refael, and T. C. H. Liew, arXiv:1409.8282.
[34] G. Panzarini, L. C. Andreani, A. Armitage, D. Baxter, M. S. Skolnick, V. N. Astratov, J. S. Roberts, A. V. Kavokin, M. R. Vladimirova, and M. A. Kaliteevski, Phys. Rev. B **59**, 5082 (1999).
[35] G. Dasbach, C. Diederichs, J. Tignon, C. Ciuti, P. Roussignol, C. Delalande, M. Bayer, and A. Forchel, Phys. Rev. B **71**, 161308 (2005).
[36] I. A. Shelykh, A. V. Kavokin, Y. G. Rubo, T. C. H. Liew, and G. Malpuech, Semicond. Sci. Technol. **25**, 013001 (2010).
[37] A. Kavokin, G. Malpuech, and M. Glazov, Phys. Rev. Lett. **95**, 136601 (2005).
[38] C. Leyder, M. Romanelli, J. P. Karr, E. Giacobino, T. C. H. Liew, M. M. Glazov, A. V. Kavokin, G. Malpuech, and A. Bramati, Nat. Phys. **3**, 628 (2007).
[39] R. Hivet, H. Flayac, D. D. Solnyshkov, D. Tanese, T. Boulier, D. Andreoli, E. Giacobino, J. Bloch, A. Bramati, G. Malpuech *et al.*, Nat. Phys. **8**, 724 (2012).
[40] S. T. Bramwell, Nat. Phys. **8**, 703 (2012).
[41] D. D. Solnyshkov, H. Flayac, and G. Malpuech, Phys. Rev. B **85**, 073105 (2012).
[42] H. Tercas, H. Flayac, D. D. Solnyshkov, and G. Malpuech, Phys. Rev. Lett. **112**, 066402 (2014).
[43] M. Galbiati, L. Ferrier, D. D. Solnyshkov, D. Tanese, E. Wertz, A. Amo, M. Abbarchi, P. Senellart, I. Sagnes, A. Lemaitre *et al.*, Phys. Rev. Lett. **108**, 126403 (2012).
[44] C. Sturm, D. Solnyshkov, O. Krebs, A. Lemaitre, I. Sagnes, E. Galopin, A. Amo, G. Malpuech, and J. Bloch, arXiv:1409.5112.
[45] V. G. Sala, D. D. Solnyshkov, I. Carusotto, T. Jacqmin, A. Lemaitre, H. Tercas, A. Nalitov, M. Abbarchi, E. Galopin, I. Sagnes *et al.*, arXiv:1406.4816.
[46] E. McCann and V. I. Fal'ko, Phys. Rev. Lett. **96**, 086805 (2006).
[47] P. Rakyta, A. Kormányos, and J. Cserti, Phys. Rev. B **82**, 113405 (2010).
[48] G. Dresselhaus, Phys. Rev. B **10**, 3602 (1974).
[49] See Supplemental Material at http://link.aps.org/supplemental/10.1103/PhysRevLett.114.026803 for the discussion of how tunneling is affected by the TE-TM splitting.
[50] P. R. Wallace, Phys. Rev. **71**, 622 (1947).
[51] F. D. M. Haldane and S. Raghu, Phys. Rev. Lett. **100**, 013904 (2008).
[52] M.-H. Liu, J. Bundesmann, and K. Richter, Phys. Rev. B **85**, 085406 (2012).
[53] H. Flayac, D. D. Solnyshkov, I. A. Shelykh, and G. Malpuech, Phys. Rev. Lett. **110**, 016404 (2013).
[54] D. V. Vishnevsky, H. Flayac, A. V. Nalitov, D. D. Solnyshkov, N. A. Gippius, and G. Malpuech, Phys. Rev. Lett. **110**, 246404 (2013).
[55] Z. Wang, Y. Chong, J. D. Joannopoulos, and M. Soljacic, Nature (London) **461**, 772 (2009).
[56] I. Carusotto and C. Ciuti, Rev. Mod. Phys. **85**, 299 (2013).
[57] Y. Lumer, Y. Plotnik, M. C. Rechtsman, and M. Segev, Phys. Rev. Lett. **111**, 243905 (2013).